ACS Partner Journal

Journal of the American Society for Mass Spectrometry

pubs.acs.org/jasms

Research Article

# Coupling 193 nm Ultraviolet Photodissociation and Ion Mobility for Sequence Characterization of Conformationally-Selected Peptides

Alyssa Q. Stiving, Sophie R. Harvey, Benjamin J. Jones, Bruno Bellina, Jeffery M. Brown, Perdita E. Barran, and Vicki H. Wysocki*

Cite This: *J. Am. Soc. Mass Spectrom.* 2020, 31, 2313–2320

Read Online

ACCESS | Metrics & More | Article Recommendations | Supporting Information

**ABSTRACT:** Ultraviolet photodissociation (UVPD) has emerged as a useful technique for characterizing peptide, protein, and protein complex primary and secondary structure. 193 nm UVPD, specifically, enables extensive covalent fragmentation of the peptide backbone without the requirement of a specific side chain chromophore and with no precursor charge state dependence. We have modified a commercial quadrupole-ion mobility-time-of-flight (Q-IM-TOF) mass spectrometer to include 193 nm UVPD following ion mobility. Ion mobility (IM) is a gas-phase separation technique that enables separation of ions by their size, shape, and charge, providing an orthogonal dimension of separation to mass analysis. Following instrument modifications, we characterized the performance of, and information that could be generated from, this new setup using the model peptides substance P, melittin, and insulin chain B. These experiments show extensive fragmentation across the peptide backbone and a variety of ion types as expected from 193 nm UVPD. Additionally, y-2 ions (along with complementary a+2 and b+2 ions) N-terminal to proline were observed. Combining the IM separation and mobility gating capabilities with UVPD, we demonstrate the ability to accomplish both mass- and mobility-selection of bradykinin des-Arg9 and des-Arg1 peptides followed by complete sequence characterization by UVPD. The new capabilities of this modified instrument demonstrate the utility of combining IM with UVPD because isobaric species cannot be independently selected with a traditional quadrupole alone.

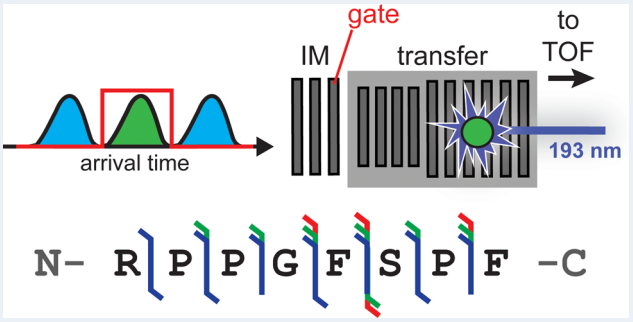




## INTRODUCTION

Proteins demonstrate significant diversity within many important biological processes. Heterogeneity can complicate analysis, but progress in mass spectrometry (MS) instrument development has driven forward the use of this technology in proteome research.[1−3] Tandem MS is routinely used to covalently fragment peptides and proteins, enabling protein identification in addition to characterizing any modifications present within a sample. Developments in activation methods have enabled faster and more in-depth protein characterization within recent years.[4−8] The most common activation method, collision-induced dissociation (CID) involves accelerating the ions of interest into a neutral background gas resulting in a stepwise buildup of internal energy and dissociation via the lowest energy pathways.[9−11] For covalent fragmentation of peptides and proteins, this typically results in the observation of predominantly b- and y-type ions.[9] While CID is easy to operate, available on virtually every commercial tandem mass spectrometer, and in many ways the "gold standard" of dissociation methods, the tendency to dissociate via these lower-energy routes can result in loss of labile post-translational modifications (PTMs) and limited sequence coverage.[12,13] Electron-based methods, such as electron-capture dissociation (ECD) and electron-transfer dissociation (ETD), result in fragments that are generated prior to energy randomization, resulting in more nonspecific fragmentation with fewer amino acid-specific cleavages and the observation of c- and z-type fragments.[7−9,14] Advantageously, electron-based methods allow the retention of PTMs and provide fragments complementary to those generated by CID.[9] However, these techniques are largely dependent on precursor charge density and, consequently, the structure of the precursor in order to accomplish effective dissociation, although combination of these techniques with collisional activation has demonstrated some success in overcoming this challenge.[15]

Ultraviolet photodissociation (UVPD) has demonstrated utility in interrogating the structure of peptides and proteins.[6,16,17] Following absorption of one or more photons, dissociation can occur via two pathways: direct dissociation

Received: July 10, 2020
Revised: September 19, 2020
Accepted: September 22, 2020
Published: September 22, 2020





https://dx.doi.org/10.1021/jasms.0c00259
*J. Am. Soc. Mass Spectrom.* 2020, 31, 2313–2320

from the excited states or internal conversion and intramolecular vibrational redistribution leading to dissociation.[9,18,19] Dissociation of peptides and proteins via UVPD leads to great diversity in fragments observed (predominantly a, b, c, x, y, and z-type fragments), enabling greater confidence in characterizing protein sequence and proteoforms.[6] Multiple wavelengths have been used for UVPD studies, each with their own advantages and disadvantages. At longer UVPD wavelengths (240−400 nm), lasers typically have a smaller footprint and do not require expensive or hazardous gases to operate, but specific chromophores are required to absorb the UV photons. At 266 nm, aromatic side chains are required, for example.[9,18] Lowering the wavelength to 193 nm, however, enables absorption of photons by the peptide backbone and removes the requirement for specific side chains.[6] Additionally, 193 nm UVPD has demonstrated extensive sequence coverage irrespective of precursor charge state.[6,20] UVPD at 157 nm has shown similar advantages to 193 nm with respect to ion types and sequence coverage (at this wavelength, excitation of most bonds is possible), but practical challenges arise with the need to transmit the entire laser beam *in vacuo*.[21,22] Both 157 and 193 nm UV lasers require larger footprints and hazardous gases ($F_2$ and ArF, respectively), but the benefits of extensive sequence information typically outweigh these challenges. The use of UVPD in top-down protein analysis has grown in recent years because of the depth of information that can be obtained about protein structure (from primary to quaternary) from this technique, including the ability to retain and localize PTMs, and ligand binding sites.[6,16,23]

Ion mobility (IM) is a useful gas-phase separation technique that enables distinction between isobaric species such as different conformations of the same $m/z$ or $m/z$-coincident oligomers.[24−27] Traveling-wave ion mobility (TWIM) involves the movement of ions through a stacked ring ion guide (SRIG) that has wave-like DC potentials and is pressurized with a neutral background gas.[28] The time it takes different ions to traverse this IM cell can be correlated with size, shape, and charge. The ability to selectively fragment different conformations of the same $m/z$ can provide insight into higher-order structural features, enabling information to be obtained about peptides and proteins beyond the primary structure.[25] Furthermore, recent work in the field of top-down protein analysis has targeted multistage dissociation to more thoroughly characterize diverse protein and protein complex systems.[23,29,30] The use of a separation and selection step between these dissociation stages enables distinction of the parent ions from which fragments are generated, and ion mobility has the distinct advantage of separating ions such as overlapping oligomeric states formed by surface-induced dissociation or ions with multiple conformations. Ion mobility is an ideal separation and selection method to combine prior to UVPD because of its ability to distinguish between such species. Using a technique known as "mobility gating", ions can be selected based on their drift times, allowing each species to then be probed with UVPD. UVPD of drift time-selected ions has been accomplished previously with 266 nm[31] and 213 nm[25] wavelengths. Here, we present the modification of a commercial instrument platform to incorporate 193 nm UVPD following IM separation and characterize its performance for a series of model peptides.

## EXPERIMENTAL SECTION

**Materials.** Substance P (sequence RPKPQQFFGLM-$NH_2$), melittin from honey bee venom (sequence GIGAVLKVLTTGLPALISWIRKRQQ-$NH_2$), insulin chain B (sequence FVNQHLC($SO_3$H)GSHLVEALYLVC($SO_3$H)GERGFFYTPKA), bradykinin des-Arg9 (1−8 fragment, sequence RPPGFSPF) acetate salt hydrate, bradykinin des-Arg1 (2−9 fragment, sequence PPGFSPFR), ubiquitin, $H_2{}^{18}O$ (97 atom % $^{18}O$), and trifluoroacetic acid (TFA) were all purchased from Sigma-Aldrich (St. Louis, MO). Peptides were dissolved in 50:50 methanol:$H_2O$ and diluted to a final concentration of 10 $\mu$M. Ubiquitin (10 $\mu$M) was used for laser beam alignment and was buffer exchanged into 100 mM ammonium acetate using Micro Bio-Spin P6 columns (Bio-Rad, Hercules, CA) prior to mass spectrometry analysis.

**Instrumentation.** A Waters Synapt G2-S mass spectrometer modified to incorporate a laser beam from an excimer laser filled with ArF gas to provide a 193 nm wavelength (ExciStar XS, Coherent, San Jose, CA), as shown in Figure S1, was used for all experiments. Many instrument modifications were made to incorporate the laser beam on the back end of the instrument similar to previous work incorporating a 213 or 266 nm laser on the back-end of this platform.[31,32] In brief, a modified lid was used to incorporate a $CaF_2$ window (Thorlabs, Inc., Newton, NJ) at the top of the time-of-flight region (manufactured by Waters Corporation). A modified pusher plate was installed within the pusher stack (manufactured by the University of Manchester machine shop) that houses a custom 45-degree (with respect to the ion beam path) fixed-angle mirror (14 mm × 6 mm × 2 mm, protected aluminum coating, $R_{max}$ @ 193 nm, 45-degree, Rocky Mountain Instrument Co., Lafayette, CO) which allows the laser beam to be reflected collinear to the ion beam. The laser beam passes through the opening (2 mm) in the tophat lens housed at the end of the transfer cell stacked-ring ion guide (SRIG) for irradiation of ions that are trapped within the transfer cell. The laser beam was aligned to the approximate center of the transfer cell. While we cannot unequivocally state that no part of the laser beam passes through the aperture of the IM exit plate, the IM data showed no indication that fragments were generated in that region.

A combination of the instrument operating software (MassLynx v4.2) and Waters Research Enabled Software (WREnS) are used to trap ions within the transfer cell and trigger the laser to fire. The trapping script used to hold ions in the transfer cell and initiate laser irradiation was modified from previous work[32] and is provided in the Supporting Information alongside a diagram of relative trapping potentials (Figure S2). Specific settings used to trap each analyte were adjusted on a case-by-case basis to minimize CID-like activation upon trapping. The laser is triggered via a spare instrument voltage and the number of laser pulses per trapping event is controlled through the number of trapping scans and laser repetition rate, as described in more detail in the Supporting Information.

Conformer-selective UVPD was accomplished by using the exit plate of the traveling-wave ion mobility (TWIM) cell as a time-controlled gate. A relatively high negative voltage (typically 20 V more negative) compared to standard operating conditions was applied to the exit plate to defocus ions (gate closed), and the standard operating voltage was applied to allow ions to pass through into the transfer cell (gate open). A diagram of relative potential voltages during the gate open and gate closed steps is provided in Figure S3. These voltages that were applied to the IM exit plate in a time-dependent manner are described in the Supporting Information.

**Experimental Workflow.** Ions were generated via nano-electrospray ionization using borosilicate capillaries that were


https://dx.doi.org/10.1021/jasms.0c00259
J. Am. Soc. Mass Spectrom. 2020, 31, 2313−2320

pulled in-house using a micropipette tip puller (Sutter Instruments model P-97, Novato, CA). A platinum wire was placed inside the solution in the capillary and a potential was applied (0.5 to 1.1 kV) to generate ions. The "sampling cone" was set to 5−10 V to minimize peptide activation, and the desired species was mass selected using the quadrupole. During UVPD-only experiments, the instrument was operated in "TOF mode" with a trap gas flow of 1−2 mL/min. During IM-UVPD experiments, the instrument was operated in "IM mode" to enable separation of ions in the TWIM cell, and a specific conformation was selected using the mobility gating procedure outlined above followed by trapping in the transfer cell. In IM-UVPD experiments, the trap gas flow was set to 1.5 mL/min, helium cell gas flow was set to 180 mL/min, and IM gas flow was set to 45 mL/min or 65 mL/min. Trap wave velocity (W.V.) was 350 m/s and wave height (W.H.) was 4 V, IM W.V. was 500 m/s and W.H. was 17 V, and transfer W.V. was 180 and W.H. was 8 V. Typical fill times were 1 s, and typical trapping times were 1 s. Typically, 5−30 laser shots with an energy of 1−3 mJ were used, as described in more detail in the relevant sections. Data were analyzed using a combination of MassLynx (v4.2, Waters Corporation, Wilmslow, U.K.), Microsoft Excel 2016 (Microsoft, U.S.A.), Protein Prospector (http://prospector.ucsf.edu, UC San Francisco), and ProSight Lite[33] (Northwestern University, Evanston, IL). UVPD and CID MS/MS spectra were internally calibrated following data collection using 3−4 high intensity, high-confidence fragment assignments (provided in Table S1). Theoretical fragments of each peptide were generated using Protein Prospector and matched to the spectra manually with a maximum error of 25 ppm.[34,35] Manually deconvoluted lists of fragment masses were also identified using ProSight Lite. Theoretical isotope distributions were generated using the isotope model tool within the MassLynx software using a full-width half-max (fwhm) that matched that of the experimental isotope patterns. Experimental and theoretical isotope distribution data sets were interpolated, and the relative ratio of each fragment type was determined using the "interp1" and "lsqminnorm" functions within Matlab (MathWorks, Natick, MA) when relevant.

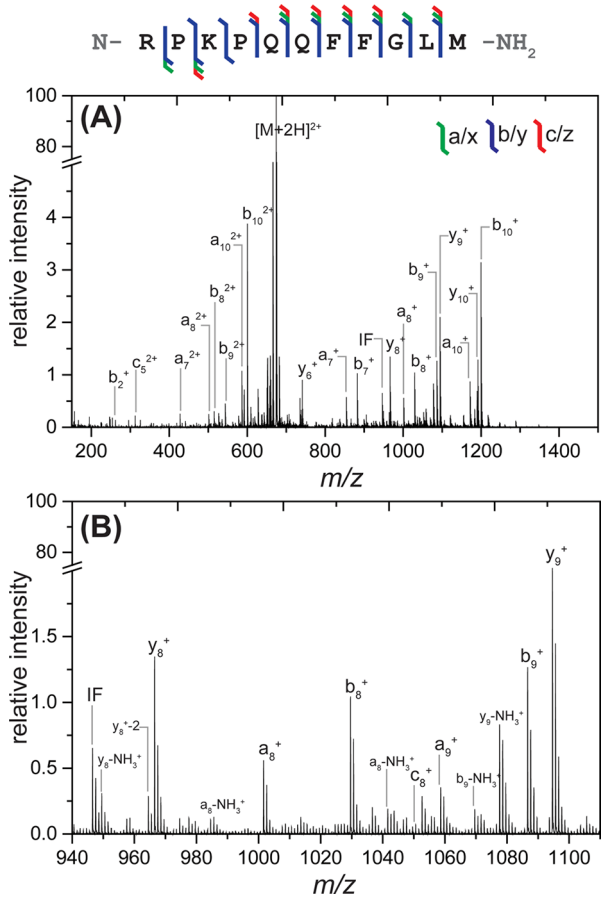


**Figure 1.** Sequence coverage map, (A) full MS/MS, and (B) zoomed-in higher $m/z$ region observed from 193 nm UVPD of substance P 2+. The isotope distribution of each fragment can be clearly resolved with good signal-to-noise as illustrated in (B). Ten laser shots at 1 mJ were used for irradiation within a 1 s trapping time. A wide variety of ion types and extensive sequence coverage were observed. Major fragments are labeled. A break is included in the $y$-axis to magnify fragment ion peaks.

## RESULTS AND DISCUSSION

**UVPD of Peptides.** Multiple model peptides were chosen to characterize instrument performance and investigate the information that could be obtained from this new instrument setup, such as sequence coverage and ion types. First, doubly charged substance P peptide ($[M+2H]^{2+}$ $m/z$ = 674) was mass selected in the quadrupole followed by trapping and 193 nm UV irradiation in the transfer cell. The resulting UVPD spectrum and sequence coverage map are shown in Figure 1A. Clear isotope distributions can be observed for each fragment ion (Figure 1B). Complementary transfer-CID and trapping-only spectra are provided in Figure S4 for comparison. The trapping script was modified to balance efficient peptide trapping while minimizing CID-like activation. Trapping of substance P demonstrated some CID-type fragments, but clear differences were observed when the peptide was irradiated. Accomplishing UVPD of this peptide using the new instrument setup described above resulted in extensive fragmentation. N-terminus fragments $a_5$−$a_{10}$, $b_2$−$b_{10}$, and $c_4$−$c_8$ were observed, whereas fewer C-terminus fragments ($x_9$−$x_{10}$, $y_8$−$y_{10}$, and $z_9$) were generated, illustrating a stronger series of N-terminus containing fragments as would be predicted given the location of the basic arginine residue (R1). Fragments that represent cleavage at every interresidue location were observed, resulting in complete (100%) sequence coverage and the observation of a variety of ion types (including a, a+1, b, c, x, y, and z-type ions). In addition to the formation of typical UVPD ion types, the unusual y-1[36] (′y), y-2 (′′y), a+2 (a′′), and b+2 (b′′) ions were also observed following irradiation of this peptide as discussed in more detail below. Internal fragments and neutral losses ($-H_2O$ and $-NH_3$) from b- and y-type ions were also observed, though there may be some influence from collisional-based activation resulting from the trapping and extraction steps. It is also worth noting that "CID-like" fragmentation (b- and y-type ions along with neutral losses) can be observed in UVPD spectra. This occurs when the energy from UV photons generates an excited electronic state which then results in internal conversion into vibrational modes followed by intramolecular vibrational distribution (IVR), which redistributes this energy throughout all available modes and subsequently results in fragmentation patterns comparable to CID.[21,37] A strong phenylalanine immonium ion ($m/z$ 120) was also observed in the low mass region of the UVPD spectra, which aligns with previous studies that show stronger abundance of immonium ions from H, W, Y, and F amino acids upon photodissociation.[38,39] The relative intensity of the F immonium ion decreased when the number of laser shots was increased,


https://dx.doi.org/10.1021/jasms.0c00259
J. Am. Soc. Mass Spectrom. 2020, 31, 2313−2320

suggesting further fragmentation, which is attributed to its higher photoabsorptivity.[38] Using 10 laser shots at 1 mJ resulted in UVPD spectra with clear isotope distributions. While comparable spectra could be obtained with a fewer number of laser shots, the S/N improved with increasing quantity of shots without causing any significant changes in ion types or sequence coverage but only causing changes in relative intensity of fragments (Figure S5).

Next, quadruply charged melittin ($[M+4H]^{4+}$ $m/z = 712$) was fragmented using the same instrument setup, and the resulting UVPD spectrum and sequence map are shown in Figure 2.

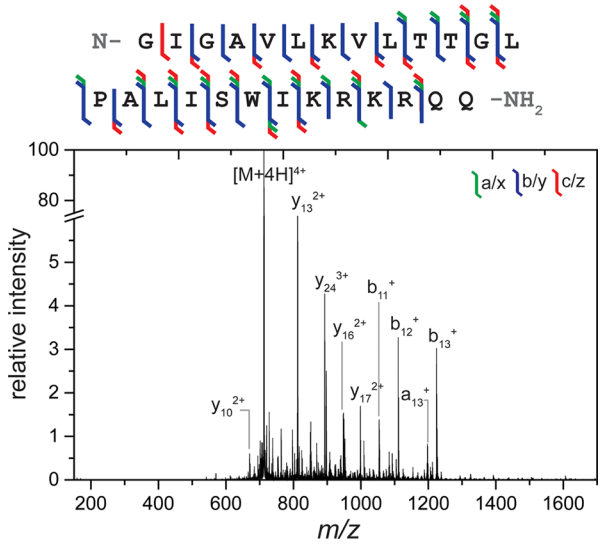


**Figure 2.** Sequence coverage map and full MS/MS spectrum observed from 193 nm UVPD of melittin 4+. Ten laser shots at 1 mJ were used for irradiation within a 1 s trapping time. A wide variety of ion types and extensive sequence coverage were observed. Major fragments are labeled. A break is included in the *y*-axis to magnify fragment ion peaks.

Complementary transfer-CID and trapping-only spectra are provided in Figure S6 for comparison. In these spectra, a slightly stronger series of C-terminus containing fragments was observed ($y_6$–$y_{24}$ and various z-type ions compared with $b_9$–$b_{24}$ and various a- and c-type ions), which is anticipated because of the location of two basic arginine residues toward the C-terminus of the melittin sequence. The UVPD spectrum of this peptide resulted in only one missed cleavage, resulting in extensive sequence coverage (96%). Similar to spectra obtained with substance P, a variety of ion types were observed. Production of the $d(a_9)^+$ fragment demonstrates the utility of 193 nm UVPD in distinguishing between isobaric residues leucine and isoleucine, though these fragments are typically observed more frequently with singly charged precursors.[38,40]

We next considered a slightly larger peptide, insulin chain B. Triply charged insulin chain B ($[M+3H]^{3+}$ $m/z$ = 1166) was fragmented using the same setup described above, and the corresponding UVPD spectrum and sequence coverage map are shown in Figure 3. Complementary transfer-CID and trapping-only spectra are provided in Figure S7. Insulin chain A and chain B are typically linked to one another with two disulfide bonds that form between C7 (chain B) and C7 (chain A) in addition to between C19 (chain B) and C20 (chain A). To study the individual chains, these disulfide bonds are oxidized and formed sulfonic acids. Including these sulfonic acid modifications on both cysteine residues, the sequence coverage obtained from

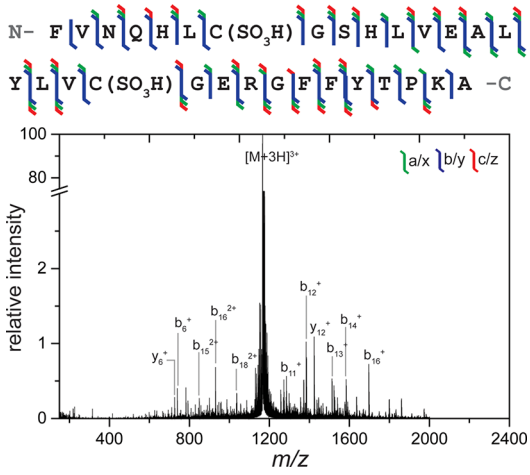


**Figure 3.** Sequence fragment map and full MS/MS spectrum observed from 193 nm UVPD of insulin chain B 3+. Ten laser shots at 1 mJ were used for irradiation within a 1 s trapping time. A wide variety of ion types and extensive sequence coverage were observed. Major fragments are labeled. A break is included in the *y*-axis to magnify fragment ion peaks.

193 nm UVPD under these experiments was 100% and demonstrated, once again, the same variety of ion types as observed for previous peptides.

**Investigation of y-1 and y-2 Fragment Ions.** After initial experiments to characterize instrument performance, it was clear that numerous y-type fragments presented different isotope distributions than expected with the presence of monoisotopic peaks at −1 Da and −2 Da mass shifts compared with the theoretical fragment monoisotopic mass. While y-1 fragments are briefly listed in some 193 nm literature,[6] to the best of our knowledge, there has been no in-depth discussion about y-2 fragments for 193 nm, although they have been discussed for 213 and 157 nm.[41,42] The identity of these fragments as y-type ions was confirmed through $^{18}O$ labeling of the C-terminus, as demonstrated in previous literature[43−45] and in more detail in the Supporting Information alongside Figure S8 and Table S2. It was determined through these labeling experiments, in combination with comparison to theoretical isotope distributions, that a mixture of y and y-1 (or, in some cases, y-2) fragments are observed rather than exclusively one ion type. When mapping the location of these unusual fragments along the peptide sequence, the observation of y-1 fragments did not show any apparent sequence-dependent trends (Figure S9). However, the y-2 fragments occurred exclusively N-terminal to proline residues (Figure S10).

Interestingly, previous work from Girod et al. (213 nm) and Kim et al. (157 nm) demonstrate the observation of these unusual y-2 fragments, alongside a+2 and b+2 complementary ions at the same location, N-terminal to proline.[41,42] Both Girod et al. and Kim et al. utilized UVPD experimental findings coupled with molecular dynamics simulations to propose mechanisms that involve homolytic bond cleavage followed by electron and hydrogen rearrangements.[41,42] The observation of y-2, a+2, and b+2 ions in these works all occurred alongside the "typical" y-, a-, and b-type fragments. In the work presented here, the comparison of experimental data to theoretical isotope distributions also demonstrate the presence of both y and y-2 fragments when utilizing 193 nm UVPD, as illustrated in Figure S11 and S12. Again similar to previous studies,[41,42] a+2 and b+2 fragments complementary to the observed y-2 ions were


https://dx.doi.org/10.1021/jasms.0c00259
J. Am. Soc. Mass Spectrom. 2020, 31, 2313−2320

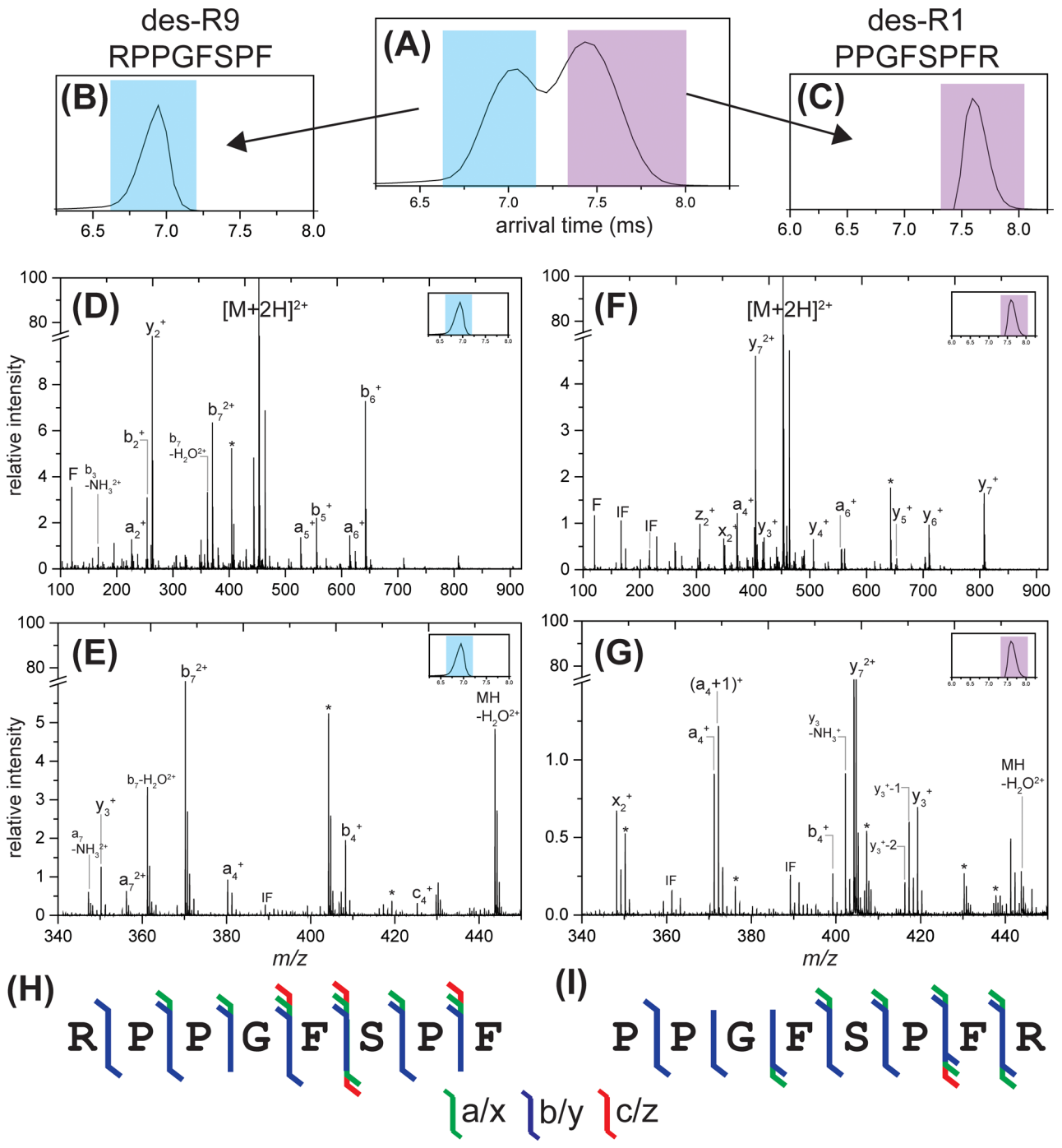


**Figure 4.** IM-UVPD of bradykinin des-Arg1/des-Arg9. (A) Arrival time distribution (ATD) of bradykinin des-Arg9 (blue) and des-Arg1 (purple) mixture from separation within the TWIM cell. The $m/z$ of each species is the same so they are unable to be separated by traditional mass analysis. (B) Bradykinin des-Arg9 and (C) bradykinin des-Arg1 show the corresponding ATDs of the drift time-selected peptides using mobility gating. Following mobility gating, the peptides were individually trapped within the transfer SRIG and irradiated with the 193 nm laser, resulting in (D) full MS/MS spectrum and (E) zoomed-in spectrum of mobility-selected bradykinin des-Arg9 alongside (F) full MS/MS spectrum and (G) zoomed-in spectrum of mobility-selected bradykinin des-Arg1. (H,I) The corresponding sequence coverage maps for UVPD of bradykinin des-Arg9 and des-Arg1, respectively. A break is included in the $y$-axis to magnify fragment ion peaks. Peaks resulting from laser noise or fragments arising from UVPD the non-mobility-selected peptide because of lack of IM baseline resolution are marked with an asterisk (*).

typically observed in experiments accomplished with 193 nm UVPD here. Comparison to theoretical isotope distributions confirm these fragments; they are clearly observed even when varying the number of laser shots or laser energy (Figure S13 and S14 demonstrate melittin $a_{13}$+2 as an example). The single exception was the lack of the $b_{13}$+2 ion for the melittin peptide. Our work here with 193 nm UVPD agrees well with these previous findings at other UV wavelengths, but additional studies will need to be conducted utilizing a more systematic investigation of peptides with and without proline to confirm these initial observations. While sequence coverage determined from 193 nm UVPD of proteins and protein complexes has shown little-to-no charge state dependence, future work will also



https://dx.doi.org/10.1021/jasms.0c00259
J. Am. Soc. Mass Spectrom. 2020, 31, 2313−2320

explore the potential impact of precursor charge state on fragmentation efficiency and patterns.[6,20]

**UVPD of Conformationally Selected Peptides.** Following successful fragmentation of mass-selected peptides with 193 nm UVPD on a Q-IM-TOF, we optimized a mobility gating method to conformationally select ions prior to UV irradiation. Mobility gating has been accomplished on the Synapt platform previously using a grounded exit plate and the MassLynx look up table function,[31] but this setup limits the amount of activation that can be accomplished pre-IM (e.g., CID or SID) because of limits on voltages in the front-end instrument optics. Here, we have applied an external voltage to the exit plate that can be adjusted for "gate open" (ions pass through the IM exit) or "gate closed" (ions are defocused at the IM exit) enabling nearly identical mobility gating operation but with increased flexibility in pre-IM activation capabilities for future experiments. First, bradykinin des-Arg9 was used to explore the mobility gating isolation widths possible with this setup by applying a voltage to the IM exit plate rather than grounding as in Bellina et al. and Theisen et al.[31,32] Using varying pulse output widths on the pulse/delay generator, the ATD width can be adjusted to be wider or narrower, as illustrated in Figure S16A−F. A pulse width of 0.05 ms corresponds to an observed ATD with a width of approximately 0.3 ms. These ions can then be trapped and irradiated with the laser and result in clear UVPD fragments (Figure S15G−J), even at narrower mobility gating widths (Figure S15J), although the signal is decreased because of the isolation of fewer ions. The ATD width that can be selected also depends on the "gate open" and "gate closed" voltages applied using the high-voltage pulser, in which a greater difference between the two can result in narrower ATD selections, but with an increased influence of CID contamination.

To demonstrate this IM-UVPD setup, we chose bradykinin des-Arg1 (PPGFSPFR) and bradykinin des-Arg9 (RPPGFSPF) peptides mixed together in solution. These peptides are variants of the bradykinin peptide, where a single arginine residue is absent from each. While their amino acid sequences differ from one another by the location of arginine, they have identical masses and therefore present at the same $m/z$. In these experiments, the doubly charged bradykinin des-Arg1 and des-Arg9 peptides were mass selected in the quadrupole ($[M+2H]^{2+}$ $m/z = 452$). Because of differences in their conformations, these two peptides can be separated from one another using IM as illustrated in Figure 4A. Following mass selection, each individual peptide was conformationally selected using mobility gating (Figure 4B for the higher mobility peptide identified as des-Arg9 and Figure 4C for the lower mobility peptide identified as des-Arg1), trapped in the transfer cell, and irradiated with the 193 nm UV laser. Because of the lack of baseline resolution in IM, the front end of the first ATD peak and back end of the second ATD peak were selected for further analysis. The corresponding MS/MS spectra for each peptide are illustrated in Figure 4D,E for des-Arg9 and des-Arg1, respectively. Highlights of the low-$m/z$ regions are shown in Figure 4F,G. Sequence maps and ion types observed for each peptide following fragmentation by UVPD are shown in Figure 4H,I. Complementary data for transfer-CID of the bradykinin des-Arg9 and des-Arg1 peptides is shown in Figure S16.

As anticipated, the MS/MS spectra from UVPD of the bradykinin des-Arg9 peptide demonstrate a strong b-ion series due to the basic arginine on the N-terminus as illustrated by high intensity b-type fragments and a complete b-type ion series. Comparably, the MS/MS spectra from UVPD of the bradykinin des-Arg1 peptide demonstrate a strong y-ion series due to the basic arginine on the C-terminus as illustrated by high intensity y-type fragments and a complete y-type ion series. The complete sequence information determined from UVPD of each peptide allows unambiguous assignment of the peptide responsible for each peak observed in the ATD. Using the same number of laser shots and the same laser pulse energy, the relative intensity of fragments occurring from the bradykinin des-Arg9 peptide was much greater (~5×) than the relative intensity of fragments generated from the des-Arg1 peptide. The CID of these peptides illustrates a similar trend; greater CID energy is required to obtain comparable precursor depletion of the des-Arg1 peptide when compared to des-Arg9, which agrees with previous work fragmenting these singly charged peptides using both CID and SID in which higher energy collisions are required to obtain comparable precursor depletion of des-Arg1 when compared to des-Arg9.[46−49] Despite a more compact conformation according to the arrival times, the observed higher-intensity fragments of the des-Arg9 peptide for identical UVPD settings is somewhat counterintuitive but can be explained by the mobile proton model. The doubly charged bradykinin des-Arg9 has one proton sequestered to the basic arginine side chain on the N-terminus, whereas the second proton is more mobile, resulting in fragmentation that can occur more easily from IVR. In contrast, the doubly protonated bradykinin des-Arg1 has one proton sequestered at the basic arginine, and the other is localized to the next most basic site at the secondary amine of Pro at the N-terminus, resulting in a higher onset energy required for fragmentation by IVR.[46]

The IM-UVPD experiments discussed here demonstrate the ability to effectively deconvolute MS/MS spectra for $m/z$-coincident species. This capability can be useful in elucidating the fragments generated from different peptide or protein conformations as demonstrated here and future work will focus on implementing this technology to deconvolute fragments generated from $m/z$-coincident oligomers of homomeric protein complexes (e.g., those produced by SID).

## CONCLUSIONS

We have demonstrated modification of a commercial ion mobility mass spectrometer to accomplish 193 nm UVPD in the transfer cell region, enabling mass-selected UVPD or conformationally selected IM-UVPD of ions. The spectra generated from this new instrument setup show significant fragmentation as illustrated by complete or nearly complete sequence coverage of model peptides without the requirement of specific side chain chromophores. Many fragment ion types were observed including a, a+2 (a′′), b, b+2 (b′′), c, d, x, y, y-1 (′y), y-2 (′′y), and z ion types. We also report the observation of y-2 fragments and the complementary a+2 and b+2 ions at interresidue cleavages N-terminal to proline, aligning with previous work from 213 and 157 nm UVPD.

Combining ion mobility separation with this UVPD setup enables ions to be irradiated following a drift time selection step, allowing for effective deconvolution of MS/MS spectra from isobaric species that cannot be separated with mass selection alone. The mobility gating setup utilized here enables full functionality of front-end activation methods. We demonstrated the utility of IM-UVPD using a mixture of bradykinin des-Arg9 and des-Arg1 peptides. These peptides cannot be separated by $m/z$ but instead their mobility separation and selection prior to UVPD enabled clear characterization of the respective peptide sequences.


https://dx.doi.org/10.1021/jasms.0c00259
J. Am. Soc. Mass Spectrom. 2020, 31, 2313−2320

Potential future work includes in-depth investigation of the y-2 fragment ions with a systematic study of proline- and nonproline-containing peptides to confirm initial observations that these fragments occur exclusively N-terminal to proline residues. Additionally, the trapping efficiency in the transfer cell will be improved to enable more effective trapping and irradiation of larger analytes. Ultimately, combination of an activation method such as CID or SID in the trap cell region of this instrument along with UVPD in the transfer cell would allow for more in-depth characterization for protein complexes via CID-IM-UVPD or SID-IM-UVPD. These experiments would allow noncovalent, subunit−subunit interactions to be cleaved (by CID or SID) before sequencing of the subunits via covalent cleavage (UVPD).

## ■ ASSOCIATED CONTENT

### Supporting Information

The Supporting Information is available free of charge at https://pubs.acs.org/doi/10.1021/jasms.0c00259.

Additional experimental and instrument modification details, $^{18}O$ labeling data, complementary transfer-CID and trapping-only spectra (PDF)

## ■ AUTHOR INFORMATION


### Corresponding Author

**Vicki H. Wysocki** − *Department of Chemistry and Biochemistry and Resource for Native Mass Spectrometry Guided Structural Biology, The Ohio State University, Columbus, Ohio 43210, United States;* orcid.org/0000-0003-0495-2538; Email: wysocki.11@osu.edu

### Authors

**Alyssa Q. Stiving** − *Department of Chemistry and Biochemistry and Resource for Native Mass Spectrometry Guided Structural Biology, The Ohio State University, Columbus, Ohio 43210, United States;* orcid.org/0000-0002-9334-1212

**Sophie R. Harvey** − *Department of Chemistry and Biochemistry and Resource for Native Mass Spectrometry Guided Structural Biology, The Ohio State University, Columbus, Ohio 43210, United States;* orcid.org/0000-0003-0763-8173

**Benjamin J. Jones** − *Department of Chemistry and Biochemistry and Resource for Native Mass Spectrometry Guided Structural Biology, The Ohio State University, Columbus, Ohio 43210, United States;* orcid.org/0000-0002-6135-4377

**Bruno Bellina** − *Michael Barber Centre for Collaborative Mass Spectrometry, Manchester Institute of Biotechnology, and Photon Science Institute, University of Manchester, Manchester M1 7DN, United Kingdom*

**Jeffery M. Brown** − *Waters Corporation, Wilmslow SK9 4AX, United Kingdom;* orcid.org/0000-0001-8569-7174

**Perdita E. Barran** − *Michael Barber Centre for Collaborative Mass Spectrometry, Manchester Institute of Biotechnology, and Photon Science Institute, University of Manchester, Manchester M1 7DN, United Kingdom;* orcid.org/0000-0002-7720-586X

Complete contact information is available at: https://pubs.acs.org/10.1021/jasms.0c00259


### Notes

The authors declare the following competing financial interest(s): Jeffery Brown is an employee of Waters Corporation, which manufactures and sells Synapt G2-S instruments.

## ■ ACKNOWLEDGMENTS

The authors gratefully acknowledge funding from the National Institutes of Health (NIH P41GM128577) awarded to V.H.W. We would also like to thank Dr. Emmy Hoyes of Waters Corporation for her help with modifying and optimizing WREnS scripts.

## ■ REFERENCES


(1) Aebersold, R. A Mass Spectrometric Journey into Protein and Proteome Research. *J. Am. Soc. Mass Spectrom.* **2003**, *14* (7), 685−695.

(2) Yates, J. R. Recent Technical Advances in Proteomics. *F1000Research* **2019**, *8*, 351.

(3) Mesri, M. Advances in Proteomic Technologies and Its Contribution to the Field of Cancer. *Adv. Med.* **2014**, *2014*, 238045.

(4) Yates, J. R.; Ruse, C. I.; Nakorchevsky, A. Proteomics by Mass Spectrometry: Approaches, Advances, and Applications. *Annu. Rev. Biomed. Eng.* **2009**, *11* (1), 49−79.

(5) Zhang, Y.; Fonslow, B. R.; Shan, B.; Baek, M.-C.; Yates, J. R. Protein Analysis by Shotgun/Bottom-up Proteomics. *Chem. Rev.* **2013**, *113* (4), 2343−2394.

(6) Shaw, J. B.; Li, W.; Holden, D. D.; Zhang, Y.; Griep-Raming, J.; Fellers, R. T.; Early, B. P.; Thomas, P. M.; Kelleher, N. L.; Brodbelt, J. S. Complete Protein Characterization Using Top-Down Mass Spectrometry and Ultraviolet Photodissociation. *J. Am. Chem. Soc.* **2013**, *135* (34), 12646−12651.

(7) Zubarev, R. A.; Kelleher, N. L.; McLafferty, F. W. Electron Capture Dissociation of Multiply Charged Protein Cations. A Nonergodic Process. *J. Am. Chem. Soc.* **1998**, *120* (13), 3265−3266.

(8) Mikesh, L. M.; Ueberheide, B.; Chi, A.; Coon, J. J.; Syka, J. E. P.; Shabanowitz, J.; Hunt, D. F. The Utility of ETD Mass Spectrometry in Proteomic Analysis. *Biochim. Biophys. Acta, Proteins Proteomics* **2006**, *1764* (12), 1811−1822.

(9) Brodbelt, J. S. Ion Activation Methods for Peptides and Proteins. *Anal. Chem.* **2016**, *88*, 30−51.

(10) Sobott, F.; Watt, S. J.; Smith, J.; Edelmann, M. J.; Kramer, H. B.; Kessler, B. M. Comparison of CID Versus ETD Based MS/MS Fragmentation for the Analysis of Protein Ubiquitination. *J. Am. Soc. Mass Spectrom.* **2009**, *20* (9), 1652−1659.

(11) McLuckey, S. A. Principles of Collisional Activation in Analytical Mass Spectrometry. *J. Am. Soc. Mass Spectrom.* **1992**, *3* (6), 599−614.

(12) Paizs, B.; Suhai, S. Fragmentation Pathways of Protonated Peptides. *Mass Spectrom. Rev.* **2005**, *24* (4), 508−548.

(13) Kim, M.-S.; Zhong, J.; Kandasamy, K.; Delanghe, B.; Pandey, A. Systematic Evaluation of Alternating CID and ETD Fragmentation for Phosphorylated Peptides. *Proteomics* **2011**, *11* (12), 2568−2572.

(14) Hart-Smith, G. A Review of Electron-Capture and Electron-Transfer Dissociation Tandem Mass Spectrometry in Polymer Chemistry. *Anal. Chim. Acta* **2014**, *808*, 44−55.

(15) Ledvina, A. R.; Beauchene, N. A.; McAlister, G. C.; Syka, J. E. P.; Schwartz, J. C.; Griep-Raming, J.; Westphall, M. S.; Coon, J. J. Activated-Ion ETD (AI-ETD) Improves the Ability of ETD to Identify Peptides in a Complex Mixture. *Anal. Chem.* **2010**, *82* (24), 10068−10074.

(16) Morrison, L. J.; Brodbelt, J. S. 193 Nm Ultraviolet Photodissociation Mass Spectrometry of Tetrameric Protein Complexes Provides Insight into Quaternary and Secondary Protein Topology. *J. Am. Chem. Soc.* **2016**, *138* (34), 10849−10859.

(17) Sipe, S. N.; Patrick, J. W.; Laganowsky, A.; Brodbelt, J. S. Enhanced Characterization of Membrane Protein Complexes by Ultraviolet Photodissociation Mass Spectrometry. *Anal. Chem.* **2020**, *92* (1), 899−907.

(18) Ly, T.; Julian, R. R. Ultraviolet Photodissociation: Developments towards Applications for Mass-Spectrometry-Based Proteomics. *Angew. Chem., Int. Ed.* **2009**, *48* (39), 7130−7137.

(19) Yeh, G. K.; Sun, Q.; Meneses, C.; Julian, R. R. Rapid Peptide Fragmentation without Electrons, Collisions, Infrared Radiation, or Native Chromophores. *J. Am. Soc. Mass Spectrom.* **2009**, *20* (3), 385−393.

(20) Sipe, S. N.; Brodbelt, J. S. Impact of Charge State on 193 Nm Ultraviolet Photodissociation of Protein Complexes. *Phys. Chem. Chem. Phys.* **2019**, *21* (18), 9265−9276.
(21) Julian, R. R. The Mechanism Behind Top-Down UVPD Experiments: Making Sense of Apparent Contradictions. *J. Am. Soc. Mass Spectrom.* **2017**, *28*, 1823−1826.
(22) Thompson, M. S.; Cui, W.; Reilly, J. P. Fragmentation of Singly Charged Peptide Ions by Photodissociation at Λ=157 Nm. *Angew. Chem., Int. Ed.* **2004**, *43* (36), 4791−4794.
(23) Mehaffey, M. R.; Sanders, J. D.; Holden, D. D.; Nilsson, C. L.; Brodbelt, J. S. Multi-Stage Ultraviolet Photodissociation Mass Spectrometry to Characterize Single Amino Acid Variants of Human Mitochondrial BCAT2. *Anal. Chem.* **2018**, *90* (16), 9904−9911.
(24) Gadkari, V. V.; Harvey, S. R.; Raper, A. T.; Chu, W.-T.; Wang, J.; Wysocki, V. H.; Suo, Z. Investigation of Sliding DNA Clamp Dynamics by Single-Molecule Fluorescence, Mass Spectrometry and Structure-Based Modeling. *Nucleic Acids Res.* **2018**, *46* (6), 3103−3118.
(25) Theisen, A.; Black, R.; Corinti, D.; Brown, J. M.; Bellina, B.; Barran, P. E. Initial Protein Unfolding Events in Ubiquitin, Cytochrome c and Myoglobin Are Revealed with the Use of 213 Nm UVPD Coupled to IM-MS. *J. Am. Soc. Mass Spectrom.* **2019**, *30* (1), 24−33.
(26) Zhou, M.; Huang, C.; Wysocki, V. H. Surface-Induced Dissociation of Ion Mobility-Separated Noncovalent Complexes in a Quadrupole/Time-of-Flight Mass Spectrometer. *Anal. Chem.* **2012**, *84* (14), 6016−6023.
(27) Dixit, S. M.; Polasky, D. A.; Ruotolo, B. T. Collision Induced Unfolding of Isolated Proteins in the Gas Phase: Past, Present, and Future. *Curr. Opin. Chem. Biol.* **2018**, *42*, 93−100.
(28) Giles, K.; Pringle, S. D.; Worthington, K. R.; Little, D.; Wildgoose, J. L.; Bateman, R. H. Applications of a Travelling Wave-Based Radio-Frequency-Only Stacked Ring Ion Guide. *Rapid Commun. Mass Spectrom.* **2004**, *18* (20), 2401−2414.
(29) Wongkongkathep, P.; Han, J. Y.; Choi, T. S.; Yin, S.; Kim, H. I.; Loo, J. A. Native Top-Down Mass Spectrometry and Ion Mobility MS for Characterizing the Cobalt and Manganese Metal Binding of α-Synuclein Protein. *J. Am. Soc. Mass Spectrom.* **2018**, *29* (9), 1870−1880.
(30) Belov, M. E.; Damoc, E.; Denisov, E.; Compton, P. D.; Horning, S.; Makarov, A. A.; Kelleher, N. L. From Protein Complexes to Subunit Backbone Fragments: A Multi-Stage Approach to Native Mass Spectrometry. *Anal. Chem.* **2013**, *85* (23), 11163−11173.
(31) Theisen, A.; Yan, B.; Brown, J. M.; Morris, M.; Bellina, B.; Barran, P. E. Use of Ultraviolet Photodissociation Coupled with Ion Mobility Mass Spectrometry To Determine Structure and Sequence from Drift Time Selected Peptides and Proteins. *Anal. Chem.* **2016**, *88*, 9964−9971.
(32) Bellina, B.; Brown, J. M.; Ujma, J.; Murray, P.; Giles, K.; Morris, M.; Compagnon, I.; Barran, P. E. UV Photodissociation of Trapped Ions Following Ion Mobility Separation in a Q-ToF Mass Spectrometer. *Analyst* **2014**, *139*, 6348−6351.
(33) Fellers, R. T.; Greer, J. B.; Early, B. P.; Yu, X.; LeDuc, R. D.; Kelleher, N. L.; Thomas, P. M. ProSight Lite: Graphical Software to Analyze Top-down Mass Spectrometry Data. *Proteomics* **2015**, *15* (7), 1235−1238.
(34) Thannhauser, T. W.; Shen, M.; Sherwood, R.; Howe, K.; Fish, T.; Yang, Y.; Chen, W.; Zhang, S. A Workflow for Large-Scale Empirical Identification of Cell Wall N-Linked Glycoproteins of Tomato (Solanum Lycopersicum) Fruit by Tandem Mass Spectrometry. *Electrophoresis* **2013**, *34* (16), 2417−2431.
(35) Helm, D.; Vissers, J. P. C.; Hughes, C. J.; Hahne, H.; Ruprecht, B.; Pachl, F.; Grzyb, A.; Richardson, K.; Wildgoose, J.; Maier, S. K.; Marx, H.; Wilhelm, M.; Becher, I.; Lemeer, S.; Bantscheff, M.; Langridge, J. I.; Kuster, B. Ion Mobility Tandem Mass Spectrometry Enhances Performance of Bottom-up Proteomics. *Mol. Cell. Proteomics* **2014**, *13* (12), 3709−3715.
(36) Roepstorff, P.; Fohlman, J. Letter to the editors. *Biomed. Mass Spectrom.* **1984**, *11* (11), 601.
(37) Zabuga, A. V.; Kamrath, M. Z.; Boyarkin, O. V.; Rizzo, T. R. Fragmentation Mechanism of UV-Excited Peptides in the Gas Phase. *J. Chem. Phys.* **2014**, *141* (15), 154309.
(38) Kelkar, D. A.; Chattopadhyay, A. The Gramicidin Ion Channel: A Model Membrane Protein. *Biochim. Biophys. Acta, Biomembr.* **2007**, *1768* (9), 2011−2025.
(39) DeGraan-Weber, N.; Ashley, D. C.; Keijzer, K.; Baik, M.-H.; Reilly, J. P. Factors Affecting the Production of Aromatic Immonium Ions in MALDI 157 Nm Photodissociation Studies. *J. Am. Soc. Mass Spectrom.* **2016**, *27* (5), 834−846.
(40) Rady, I.; Siddiqui, I. A.; Rady, M.; Mukhtar, H. Melittin, a Major Peptide Component of Bee Venom, and Its Conjugates in Cancer Therapy. *Cancer Lett.* **2017**, *402*, 16−31.
(41) Girod, M.; Sanader, Z.; Vojkovic, M.; Antoine, R.; MacAleese, L.; Lemoine, J.; Bonacic-Koutecky, V.; Dugourd, P. UV Photodissociation of Proline-Containing Peptide Ions: Insights from Molecular Dynamics. *J. Am. Soc. Mass Spectrom.* **2015**, *26* (3), 432−443.
(42) Kim, T.-Y.; Valentine, S. J.; Clemmer, D. E.; Reilly, J. P. Gas-Phase Conformation-Specific Photofragmentation of Proline-Containing Peptide Ions. *J. Am. Soc. Mass Spectrom.* **2010**, *21* (8), 1455−1465.
(43) Niles, R.; Witkowska, H. E.; Allen, S.; Hall, S. C.; Fisher, S. J.; Hardt, M. Acid-Catalyzed Oxygen-18 Labeling of Peptides for Proteomics Applications. *Anal. Chem.* **2009**, *81* (7), 2804−2809.
(44) Roe, M. R.; McGowan, T. F.; Thompson, L. V.; Griffin, T. J. Targeted 18O-Labeling for Improved Proteomic Analysis of Carbonylated Peptides by Mass Spectrometry. *J. Am. Soc. Mass Spectrom.* **2010**, *21* (7), 1190−1203.
(45) Castillo, M. J.; Reynolds, K. J.; Gomes, A.; Fenselau, C.; Yao, X. Quantitative Protein Analysis Using Enzymatic [18O]Water Labeling. *Curr. Protoc Protein Sci.* **2014**, *76*, 23.4.1−23.4.9.
(46) Dongre, A. R.; Jones, J. L.; Somogyi, A.; Wysocki, V. H. Influence of Peptide Composition, Gas-Phase Basicity, and Chemical Modification on Fragmentation Efficiency: Evidence for the Mobile Proton Model. *J. Am. Chem. Soc.* **1996**, *118* (35), 8365−8374.
(47) Laskin, J.; Bailey, T. H.; Denisov, E. V.; Futrell, J. H. On the Relative Stability of Singly Protonated Des-Arg1 and Des-Arg9 Bradykinin. *J. Phys. Chem. A* **2002**, *106* (42), 9832−9836.
(48) Pratihar, S.; Barnes, G. L.; Laskin, J.; Hase, W. L. Dynamics of Protonated Peptide Ion Collisions with Organic Surfaces: Consonance of Simulation and Experiment. *J. Phys. Chem. Lett.* **2016**, *7* (16), 3142−3150.
(49) Zhou, M. *Incorporation of Surface Induced Dissociation into a Commercial Ion Mobility - Tandem Mass Spectrometer and Application of Mass Spectrometry Methods for Structural Analysis of Non-Covalent Protein Complexes*; Ph.D. Dissertation, The Ohio State University, 2013.


https://dx.doi.org/10.1021/jasms.0c00259
*J. Am. Soc. Mass Spectrom.* 2020, 31, 2313−2320